Current Research in Food Science 9 (2024) 100874

Contents lists available at ScienceDirect

Current Research in Food Science

journal homepage: www.sciencedirect.com/journal/current-research-in-food-science

Impact of butyric acid modification on the structural and functional properties of rice starch

Qiaoyan Wu [1], Yang Yang [1], Yue Xu, Bing Wang, Xiaofei Liu, Yan Wang, Guang Zhang, Xin Bian, Chunmin Ma [**], Na Zhang [*]

College of Food Engineering, Harbin University of Commerce, Harbin, 150076, China

ARTICLE INFO

Handling Editor: Dr. Quancai Sun

Keywords:
Rice starch
Butyric acid
Esterification
Multiscale structure
Functional properties
In vitro digestibility

ABSTRACT

Rice is a food with a high starch content, comprising over 75% of its composition. However, prolonged and excessive consumption of this cereal may lead to elevated blood glucose levels, which can increase the risk of obesity, type 2 diabetes, and cardiovascular disease. Butyric acid (BA), the primary energy source for colonic epithelial cells, exhibits the highest utilization rate among short-chain fatty acids, underscoring its importance for human health. In this study, rice starch butyrate (RSB) samples were synthesized using the aqueous phase process, with broken rice starch (RS) and butyric anhydride serving as the substrate. RSB samples with different degrees of substitution (DS) were produced by modulating the addition amount of butyric anhydride. The crystal structures, morphology of starch granules, pasting properties, thermal stability, and in vitro digestibilities of the RSB were investigated and compared with those of native rice starch. Fourier transform infrared (FTIR) spectroscopy confirmed the successful incorporation of butyryl into the starch molecules. With the increase in DS, the roughness of the RSB material's surface gradually increased, leading to the deterioration of the smooth structure on certain surfaces, which resulted in the appearance of cracks and collapses. Additionally, the crystallinity diminished from 24.77% to 7.41% with increasing DS. Concurrently, in vitro digestive characterisation revealed that the percentage of resistant starch increased from 24.33% to 47.72%. Thus, this study can provide a theoretical basis for the development of novel products of amyl butyrate.

1. Introduction

Rice starch (RS) is a widely used carbohydrate source, recognized for its unique properties that make it suitable for various food applications (Rostamabadi et al., 2024a, 2024b). However, the inherent limitations of natural starches, including insufficient shear stress resistance, a high degree of conversion, and low thermal stability, restrict their applicability in food products (Wang et al., 2024). Chemical modification techniques can significantly alter the structure of starch by introducing specific functional groups that interact with hydroxyl groups (Zarski et al., 2024). A notable modification technique is butyrylation, which is a type of esterification that incorporates butyric acid into the starch structure (Zhang et al., 2024). This process modifies many of the properties of starch, such as digestibility, thermal stability and pasting ability, making it an ideal candidate for a variety of industrial applications (Li et al., 2022c; Li et al., 2024).

Butyric acid (BA), a short-chain fatty acid (SCFA), is instrumental in regulating microbial metabolism and plays a crucial role in cellular energy metabolism and gut homeostasis (Portincasa et al., 2022; Yao et al., 2022). In recent years, the literature has indicated that butyric acid significantly maintains intestinal health, regulating appetite and body weight, as well as enhancing lipid metabolism and glucose homeostasis (He et al., 2020). However, the endogenous production of butyric acid by intestinal epithelial cells is often insufficient to meet physiological demands (Fu et al., 2019). Currently, butyrylated starch is recognized as a suitable and efficient alternative to butyric acid in the human body (Maiuolo et al., 2024). Numerous studies have demonstrated that the addition of butyric acid groups to starch can alter its molecular structure, significantly affecting its physical properties and functional activities (Cornejo-Ramrez et al., 2018; Egharevba, 2019).

* Corresponding author. College of Food Engineering, Harbin University of Commerce, Harbin, Heilongjiang, 150028, China.
** Corresponding author. No.1, Xuehai Street, Songbei District, Harbin, Heilongjiang Province, China.
E-mail addresses: chunmin_ma@163.com (C. Ma), foodzhangna@163.com (N. Zhang).
[1] The authors contribute equally to the work.

https://doi.org/10.1016/j.crfs.2024.100874
Received 30 August 2024; Received in revised form 20 September 2024; Accepted 1 October 2024
Available online 5 October 2024

Butyric anhydride and starch, synthesized through esterification to form butyrate starch, represent significant classes of colonic microbial carbon sources that modulate gut microbiota composition and influence short-chain fatty acid production (Cheng and Zhou, 2024). Concurrently, the targeted delivery of specific esterified butyric acid to the colon has the potential to enhance human health (Wang et al., 2019). For instance, Li et al. (2021) demonstrated that butyrylated starch can mitigate DSS-induced (dextran sulfate sodium, DSS) colitis in mice by specifically releasing butyrate in the colon and providing substrates for gut microbiota fermentation. In a subsequent study, Li et al. (2022b) explored the impact of the botanical source on the distribution of butyl groups in butyrylated starch, emphasizing its significance in modulating intestinal digestion and colon fermentation. Additionally, Li et al. (2022d) investigated the characteristics of butyrylated seed starch, focusing on the presence of butyryl groups at various carbon positions. Conversely, Zhang et al. (2024) provided a comprehensive review of the structural characteristics, digestion properties, fermentation properties, and biological activities of butyrylated starch, shedding light on its potential applications in the food industry. The relatively low allergy risk of rice compared to certain other grains, such as wheat or soy, helps to fulfill the need for allergy-friendly foods. And rice starch has good dietary compatibility for most people, especially for those with allergies to wheat or other grains. Therefore, to elucidate the mechanism by which butyric acidified rice starch affects human health, further in-depth studies on this topic are necessary.

In this work, rice starches with different substitution degrees of butyrate were prepared. The apparent morphology, molecular structure, crystal structure, and particle properties were investigated by scanning electron microscopy (SEM), Fourier transform infrared spectroscopy (FTIR), X-ray diffraction (XRD), and a Malvern laser particle sizer. On this basis, the pasting characteristics, thermal stability, and in vitro antidigestibility of butyrylated rice starch (RSB) with different substitution degrees were subsequently investigated. This will play an important role in elucidating the potential applications of RSB in functional foods and dietary supplements.

2. Materials and methods

2.1. Materials

Broken rice was sourced from Jinhe Rice Industry Co., Ltd. (Wuchang, China). Butyric anhydride (AR, 99.7%) was obtained from Shanghai Aladdin Biochemical Technology Co., Ltd. (Shanghai, China). α-Amylase (BR, 4000 U/g) was procured from Sigma-Aldrich (St. Louis, Missouri, USA). Amyloglucosidase (BR, 260 U/mL) and dimethyl sulfoxide (AR, 99.9%) were supplied by Shanghai McLean Biochemical Technology Co., Ltd. (Shanghai, China). The glucose peroxidase (GOPOD) test kit was acquired from Leadman Biochemistry Co., Ltd. (Nanjing, China). All remaining reagents and solutions were of analytical grade and required no further purification.

2.2. Preparation of butyrylated rice starch

The rice was crushed and passed through an 80-mesh sieve, stirred in 4 g/L NaOH for 4 h, centrifuged at 4000×*g* for 15 min, and the supernatant and the yellow soft layer were discarded, re-dissolved and centrifuged again. The process was repeated three times. Finally, the pH was adjusted to 7.0 with 1.0 mol/L HCl, and then centrifuged again, and the resulting starch was dried at 45 °C for 24 h and passed through a 100-mesh sieve.

A precise quantity of broken rice starch was weighed and dissolved in distilled water to prepare a 40% starch emulsion. Subsequently, varying amounts of butyric anhydride were incrementally introduced over a 30 min, accompanied by the addition of 1.0 mol/L NaOH to maintain the pH of the solution within the range of 8.0–8.7. The reaction was conducted at a temperature of 40 °C for a period of 4 h. Upon completion, the emulsion was acidified to a pH of 6.0 using 1.0 mol/L HCl, followed by centrifugation (4000 g) for 10 min at 4 °C. The resultant product was then washed three times with distilled water and ethanol to eliminate any residual butyric anhydride. The samples were dried in an oven at 45 °C for 24 h and stored.

2.3. Determination of substitution degree (DS)

The procedure was modified in accordance with the earlier study (Dong et al., 2023). Weigh 2.5 g of rice starch with butyrate in a beaker, add 50 mL of distilled water, and mix with a magnetic stirrer. The saponification process was then carried out by adding 25 mL of sodium hydroxide solution (0.5 mol/L) and rapidly stirring at a high speed for 30 min, all the while adding 5 drops of phenolphthalein indicator. Finally, a 0.2 mol/L HCl standard solution was used to titrate the excess base in the sample, and the pink simply vanished at the conclusion of the titration process. At the same time, a blank experiment with untreated broken rice starch was conducted. The following formula was used to compute the DS:

$$\omega = \frac{(V_1 - V_0) \times c \times M}{m \times 1000} \times 100\%$$

$$DS = \frac{162 \times \omega}{7100 - 70 \times \omega}$$

where m is the sample weight, g; 162 is the relative molecular mass of the dehydrated glucose unit; c is the concentration of HCl standard solution, mol/L; ω is the mass fraction of butyryl groups contained in each glucose unit of the butyrate starch; V_1 is the volume of HCl standard solution consumed by the blank sample; and V_0 is the volume of standard solution of HCl consumed by butyrate rice starch.

2.4. Amylose content

A modified version of the Dhull et al. (2021) approach was used to ascertain the amylose content of RSB. A moderate amount of alcohol (100 mL), sodium hydroxide solution (900 μL), and starch samples (10 mg) were combined. After 10 min of boiling in water, the mixture was allowed to cool, fixed to 10 mL, and then left to be measured. 10 mL dilution was applied to the 0.5 mL test solution, 0.1 mL acetic acid, and 0.2 mL potassium iodide solution. At room temperature, the absorbance was measured at 620 nm after 10 min. The following formula was used to determine the straight chain starch content:

$$\text{Amylose content } (\%) = \frac{C}{M} \times 10$$

where M is the starch weight, 10 is the correction factor, and C is the result computed from the standard curve.

2.5. Particle size analysis

The butyrate rice starch particle size was analysed using the light scattering technique (mode of Dx (50)). After being dissolved in 1% (w/v) of H_2O, raw starch granules were introduced to the device and stirred cyclically at high speed. Using the general analytical model in the Mastersizer analysis program, the refractive index and absorption index of the granules were examined. The dispersant water's refractive index was 1.33, whereas the absorption and refractive indices were 1.53 and 0.1, respectively (Li et al., 2022b).

2.6. Fourier transform infrared spectroscopy (FTIR) analysis

FTIR spectroscopy (4000–400 cm^{-1}) was used to characterise the samples' material structure and confirm the presence of certain bands throughout the butyrylation process. The starch ester and potassium

bromide were crushed in a quartz mortar at a mass ratio of 1:500, loaded into a mold and pressed into a collector to scan the samples. These were the settings for the measuring parameters: resolution of 4 cm^{-1}, scan range of 4000 cm^{-1}-400 cm^{-1}, scan times of 64 times, and a half peak width of 47 cm^{-1} and an enhancement factor of 3.0 were the parameter requirements for using OMNIC 8.0 to deconvolute the peaks in the range of 1200 cm^{-1}-900 cm^{-1}. Ultimately, peak splitting of the spectra using Peak Fit software produced peak intensities of 1047 cm^{-1} and 1022 cm^{-1}.

2.7. X-ray diffraction (XRD) analysis

The starch samples prepared above were pulverized and passed through a 120 mesh sieve, and the crystal structure of RSB was determined by XRD. The test method's particular parameters were as follows: Cu-Kα radiation (λ = 0.25 nm) with a bragg angle (2θ) ranging from 5° to 60° and a scanning speed step of 0.02°/min. Peak Fit software was used for the analysis of the XRD diffraction patterns.

2.8. Scanning electron microscopy (SEM) analysis

The following was the experimental procedure used to observe butyrate rice starch using an SEM. A trace amount of the sample was glued to the surface of a suitable copper stage with conductive adhesive, and a suction ear ball was used to remove the unfixed sample to prevent a large amount of agglomerated starch sample. A sputter coater was used to coat the samples with gold to create conductive samples. Images were taken at an accelerating voltage of 5.00 kV, and the apparent morphology of the starch esters was observed at magnifications of 2500 and 5000 times, respectively.

2.9. Pasting properties (RVA) analysis

The Liu et al. (2019) approach was cited, with a little adjustment. A Rapid Viscosity Analyser (S4, Newport Scientific, US) aluminium canister held 3 g of carefully measured RSB. The software that came with the sample was used to determine its specific moisture content. The experiment's setup included an initial temperature hold at 50 °C, followed by a 5 °C/min all the way up to 95 °C. After holding the sample at 95 °C for 7 min, the test was completed by cooling it back down to 50 °C at the same pace.

2.10. Diffevential scanning calorimetry (DSC) analysis

Employing a differential scanning calorimeter, the thermodynamic characteristics of butyrylated rice starch were ascertained. The device was calibrated using indium as a reference and nitrogen as a protective gas. Precisely weigh 3 mg of sample powder in an aluminium DSC crucible. Add deionised water at a ratio of 1:2 (w/v, sample dry basis), and let to equilibrate for a full day. As a control, a blank aluminium DSC crucible was used. Each sample was tested three times in parallel, with the temperature range being 20–125 °C, the heating rate being 10 °C/min, and the nitrogen flow rate being 20 mL/min. The device's software evaluated the samples' thermodynamic parameters, such as their start temperature (T_0), peak temperature (T_p), end temperature (T_c), and enthalpy (ΔH).

2.11. In vitro digestion

The simulated in vitro digestion approach described by Xie et al. (2019) was used to study the digestive characteristics of butyrate rice starch. Combine 1 mL of amyloglucosidase (100,000 U/mL) and 0.16 g of porcine pancreatic α-amylase (50,000 U/g) in phosphate buffer and store as a mixed enzyme reserve. 10 mL of $C_2H_5NaO_2$ (pH 5.2) were added to a test tube containing 200 mg RSB. After heating the aforementioned samples for 20 min in a boiling water bath, 10 mL of the enzyme mixture was added, and they were shaken for 0, 20, 40, 60, 90, and 120 min at 37 °C, respectively. 0.5 mL of sample and 0.5 mL of anhydrous ethanol were added at each time point to inactivate the enzyme for 1 min. The glucose oxidase method was subsequently employed to quantify the sugar content following the dilution of each 1 mL sample with 4 mL of distilled water. Absorbance was measured at 510 nm after the addition of 3.0 mL of GOPOD reagent to 0.1 mL of the sample solution, which was then incubated at a temperature range of 40–50 °C for 20 min. The formula used for this determination is as follows:

$$RDS(\%) = \frac{(G_{20} - G_0)}{TS} \times 0.9 \times 100$$

$$SDS(\%) = \frac{(G_{120} - G_{20})}{TS} \times 0.9 \times 100$$

$$RS(\%) = \frac{TS - (SDS + RDS)}{TS} \times 0.9 \times 100$$

where the glucose (mg) released in T, 0, 20, and 120 min are represented by the symbols G_T, G_0, G_{20}, and G_{120}. The weight of the amylose ester is represented by TS.

2.12. Data processing and analysis

Each experiment was conducted in triplicate, and the results were expressed as the mean ± standard deviation. To assess the variability among the experimental data, a one-way analysis of variance (ANOVA) was performed using SPSS version 20.0. Data analysis with the Tukey test indicated a statistically significant difference ($p < 0.05$). The graphical representation of the experimental outcomes was generated using Origin 2024.

3. Results and discussion

3.1. DS and amylose content analysis

The degree of substitution (DS) serves as a crucial indicator of the extent of the starch esterification reaction (Cuenca et al., 2020). Table 1 demonstrated the variations in butyryl content and DS of butyrate starch with the addition of various concentrations of butyric anhydride. As the amount of butyric anhydride provided increased from 1% to 30%, the total degree of substitution for butyrylated starch rose from 0.047 to

Table 1
Structural parameters of butyrylated rice starch with different degrees of substitution.

Samples	BA concentration (%)	Butyry (%)	DS	Amylose content (%)	Dx (50)/ μm
RS	0	0	0	18.37 ± 0.35^{f}	6.083 ± 0.336^{j}
RSB-1	1	2.023 ± 0.337^{f}	0.047 ± 0.008^{f}	18.63 ± 0.12^{e}	7.479 ± 0.274^{f}
RSB-2	5	2.874 ± 0.221^{e}	0.068 ± 0.005^{e}	18.95 ± 0.11^{d}	8.724 ± 0.328^{e}
RSB-3	10	4.011 ± 0.351^{d}	0.097 ± 0.011^{d}	20.07 ± 0.20^{c}	10.484 ± 0.462^{d}
RSB-4	15	5.486 ± 0.318^{c}	0.134 ± 0.005^{c}	21.32 ± 0.21^{c}	12.637 ± 0.298^{c}
RSB-5	20	5.953 ± 0.389^{c}	0.147 ± 0.007^{c}	22.65 ± 0.19^{b}	15.449 ± 0.195^{b}
RSB-6	25	6.692 ± 0.096^{b}	0.167 ± 0.007^{b}	23.74 ± 0.21^{a}	17.724 ± 0.328^{b}
RSB-7	30	8.121 ± 0.570^{a}	0.206 ± 0.008^{a}	24.26 ± 0.15^{a}	19.723 ± 0.309^{a}

The values correspond to the mean ± standard deviation (n = 3). Different letters in the same column indicate significant differences ($P < 0.05$).

0.206. The degree of substitution exhibited a positive correlation with the availability of butyric anhydride, measured on a starch dry weight basis. It has been suggested that an increase in the concentration of reactants enhances the utilization of butyric anhydride molecules in proximity to the hydroxyl groups of starch molecules. In a similar vein, Dong et al., (2023) reported that a greater addition of butyric anhydride corresponds to an accelerated rate of the butyrylation reaction, a finding that aligns with the results of the current experiment.

Furthermore, the amylose content significantly influences the physicochemical and functional properties of starch (Sinhmar et al., 2023; Cornejo-Ramírez et al., 2018). RS exhibited an amylose content of 18.37%, whereas RSB samples demonstrated a range from 18.63% to 24.26% as the DS values increased. The process of esterification disrupted the terminal chains of the branched starch structure, resulting in the formation of shorter amylose chains and an overall increase in amylose content. These observations align with the findings of Gao et al. (2021), who reported that the amylose concentration in modified starches increased with higher DS values.

3.2. Particle size analysis

One of the most significant indicators of starch quality is the particle size distribution, which is determined by the proportion of particles of various sizes within the sample (Rostamabadi et al., 2024). The value of Dx (50) indicates that 50% of the particles are smaller than this diameter. The results demonstrated an increase in particle size from 6.083 μm to 19.723 μm with a gradual increase in substitution (Table 1). The mean particle size of esterified starch was significantly greater than that of RS, consistent with recent findings (Xu et al., 2023). During the esterification reaction, the butyryl acid group was incorporated into the starch molecule, leading to the disruption of some hydrogen bonds (Li et al., 2024). Some literature indicated that the introduction of butyl groups during esterification creates voids within the starch structure, thereby enhancing the water absorption and swelling properties of the modified starch compared to the native starch (Portillo-Perez et al., 2024). Consequently, when assessing the particle size of starch using distilled water as a medium, it was observed that the particle sizes of the RSB were frequently larger than those of the unmodified starch. This was in agreement with the study's findings.

3.3. FTIR analysis

The FTIR spectra of the RS and RBS samples, characterized by varying degrees of substitution, were presented in Fig. 1. The prominent hydroxyl peaks observed in the range of 3000–3600 cm^{-1} for native starch were attributed to the complex telescopic vibrations of both inter- and intramolecular free hydroxyl groups (Diop et al., 2011). The band observed at 2930 cm^{-1} corresponds to C-H bond stretching vibrations. As shown in Fig. 1, the characteristic peaks associated with hydroxyl groups in the starch molecules exhibit a gradual attenuation. The hydroxyl groups in rice starch were substituted with butyryl groups through a transesterification process involving butyric anhydride. Compared to the native starch, the ester carbonyl absorption peak emerged at 1726 cm^{-1} (indicated by a black arrow) (Di et al., 2016). Simultaneously, the hydroxyl group absorption peak around 3300 cm^{-1} in the butyrate-modified rice starch gradually diminished, indicating a chemical reaction between the hydroxyl groups and butyric anhydride. Previous research had demonstrated that the C=O stretching vibrations, which appeared in the range of 1720–1740 cm^{-1}, are indicative of the presence of acetyl groups. This observation aligns with the findings of this study, which identified the formation of a novel characteristic peak of ester carbonyl at 1726 cm^{-1} (indicated by the black arrow) in butyrate-modified rice starch. Additionally, the results demonstrated that the butyryl group exhibits favorable interactions with the starch molecule, as evidenced by a reduction in the intensity of -OH absorption in the starch and the appearance of new C=O bands.

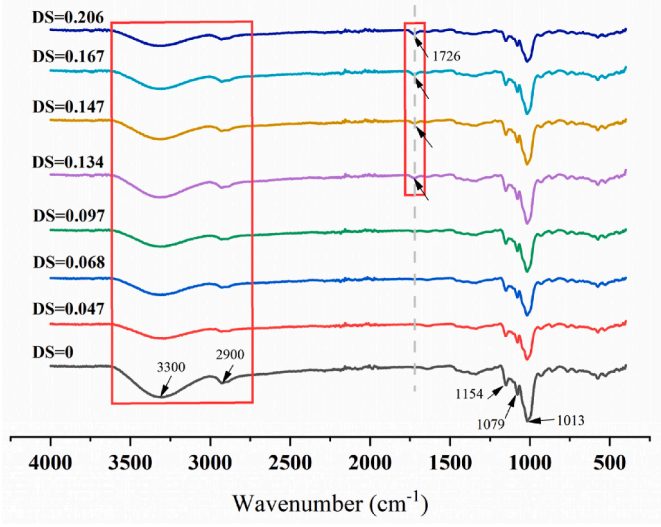

Fig. 1. FTIR spectra of natural (RS) and butyrylated (RSB) starches.

The feature peak intensity at 1013 cm^{-1} in butyrylated rice starch was significantly weaker than in natural starch, suggesting a change in the conformation of the modified rice starch. The 1047/1022 cm^{-1} and 1022/995 cm^{-1} peak ratios reveal the degree of short-range ordering in the outer regions of starch granules. As shown in Table 2, the $R_{1047/1022}$ values of butyrate rice starch showed an overall increasing trend with increasing degree of substitution, while the $R_{1022/995}$ values showed a decreasing trend. The ratio at 1047/1022 cm^{-1} for butyrylated starch exhibited an increase as the degree of substitution increased, corroborating findings from previous studies (Chen et al., 2024a). This observation suggests that acylated starch possesses a more ordered short-term structure compared to native starch.

3.4. XRD analysis

It is a standard practice to utilize X-ray diffraction (XRD) patterns to elucidate the crystalline structural characteristics of starch granules (Ma and Boye, 2018). The XRD spectra of resistant starch and butyrylated resistant starch with varying levels of substitution were presented in Fig. 2. The characteristic diffraction peaks of the A-type crystalline structure were observed at 15°, 17°, 18°, and 23°, consistent with earlier research findings. As illustrated in Fig. 2, rice starch exhibits a characteristic A-type diffraction peak (Cao et al., 2020). The X-ray diffraction patterns of butyrylated starch revealed no significant alterations in peak positions relative to unbutyrylated starch; however, the intensity of the crystallographic diffraction peaks at their respective positions was diminished. This observation suggests that the various acid esterification treatments employed in this study did not alter the crystalline structure of rice starch. This phenomenon might be attributed to the

Table 2
The effect of esterification treatment on the short-range ordered structure of starch.

Samples	$R_{1047/1022}$	$R_{1022/995}$
RS	1.233 ± 0.003^{f}	0.833 ± 0.002^{d}
RSB-1	1.236 ± 0.004^{e}	0.981 ± 0.001^{d}
RSB-2	1.207 ± 0.004^{e}	0.890 ± 0.004^{bc}
RSB-3	1.151 ± 0.002^{d}	0.892 ± 0.003^{b}
RSB-4	1.208 ± 0.001^{b}	0.901 ± 0.003^{c}
RSB-5	1.198 ± 0.002^{ab}	0.934 ± 0.001^{b}
RSB-6	1.176 ± 0.005^{a}	0.846 ± 0.004^{a}
RSB-7	1.130 ± 0.001^{a}	0.797 ± 0.002^{a}

Different superscript letters indicate that the values in each column are significantly different ($p < 0.05$).

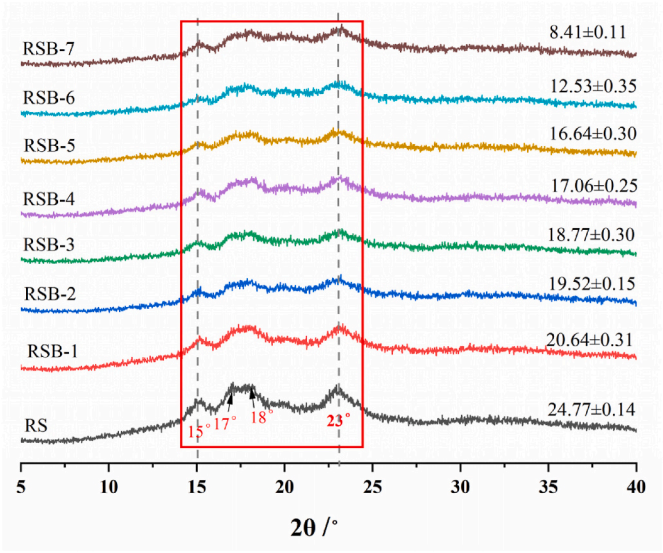

Fig. 2. XRD patterns of rice starch (RS) and butyrate rice starch (RSB) samples with different BA concentration.

partial substitution of the three active hydroxyl groups on the starch's glucose units with butyryl groups during esterification, which disrupted the hydrogen bonding interactions both between and within the original starch molecules. As the degree of substitution increased, the intermolecular forces among the starch molecules diminished, resulting in a more loosely packed structure. The relative crystallinity exhibited a gradual decline from 24.77% to 8.41% with increasing substitution. This observation aligns with findings reported by Ali and Hasnain (2016), which attributed the degree of starch crystallization primarily to the formation of double helices through intermolecular hydrogen bonding within branched starch fragments. Additionally, the partial substitution of hydroxyl groups and the consequent reduction in both intermolecular and intramolecular hydrogen bond formation during acylation further contributed to the observed decrease in starch crystallinity.

3.5. Morphological observation

The incorporation of butyl groups markedly influenced the morphology of starch granules. Fig. 3 presented SEM images of RS and RSB with varying degrees of substitution. The surface of native rice starch granules appeared relatively smooth, devoid of conspicuous cracks or fractures, and predominantly exhibited irregular shapes with sharp angles and edges. In contrast, the morphology and dimensions of the butyrylated starch granules, specifically RSB-1 and RSB-2 with lower DS, remained largely unchanged compared to the native rice starch. However, certain surfaces exhibited a loss of their smooth structure, with the epidermis peeling off to form grooves, and the starch granules beginning to aggregate. These observations are consistent with the findings of several other studies (Dai et al., 2019; Espinosa-Solis et al., 2020). As the degree of substitution increases, aggregation and agglomeration of starch ester granules (RSB-3) commence. When the DS reaches 0.147, cracks and collapses become evident on the surface of the starch ester granules. This phenomenon was attributed to the infiltration of low concentration esterifying agents into the starch granules, where they reacted with the hydroxyl groups of the starch. This interaction resulted in some disruption of the surface structure of the starch granules. As the DS of the acylated starch increased, a loss of the original granule morphology was observed and the granules were reorganized into larger, irregularly shaped aggregates. Shi et al. (2022) reported that octenylsuccinic acid induces a certain degree of damage to the surface of starch granules. Furthermore, with an increase in the degree of substitution, starch exhibited a tendency towards agglomeration, a finding that aligns with the results presented in this work. In summary, the DS was positively correlated with the appearance of partially broken starch and the extent of surface destruction on RSB particles.

3.6. Pasting properties

The thermal process of starch paste gelatinization involves the exposure of starch granules to an aqueous solution, resulting in water absorption and subsequent swelling. During this process, intramolecular hydrogen bonds are disrupted, leading to the partial dissolution of starch molecules (Guo et al., 2024). Table 3 displayed the pasting parameters for butyric acid starch esters with varying degrees of substitution. The esterification of starch notably decreased its peak viscosity from 2687.0 cP to 1054.3 cP, in comparison to the native rice starch. Butyric acid interacts with starch, resulting in the formation of new chemical groups that enhance the interaction between butyric acid molecules and rice starch molecules. This interaction facilitates cross-linking and the formation of ester bonds, which inhibit the pasteurization reaction by increasing the spatial resistance of water molecules, thereby reducing the viscosity of the modified starch (Zhao et al., 2018). The disintegration value serves as an indicator of the degree of thermal stability and the extent of starch granule degradation upon heating (Su et al., 2020). The disintegration values for rice starch ester butyrate were significantly reduced (669.0 cP to 103.7 cP), indicating that the starch granules exhibited enhanced structural integrity post-dissolution and increased thermal stability following esterification. The regrowth value, indicative of the extent of recrystallization during the cooling phase of the starch paste, serves as a measure of the starch's aging process (Jiang et al.,

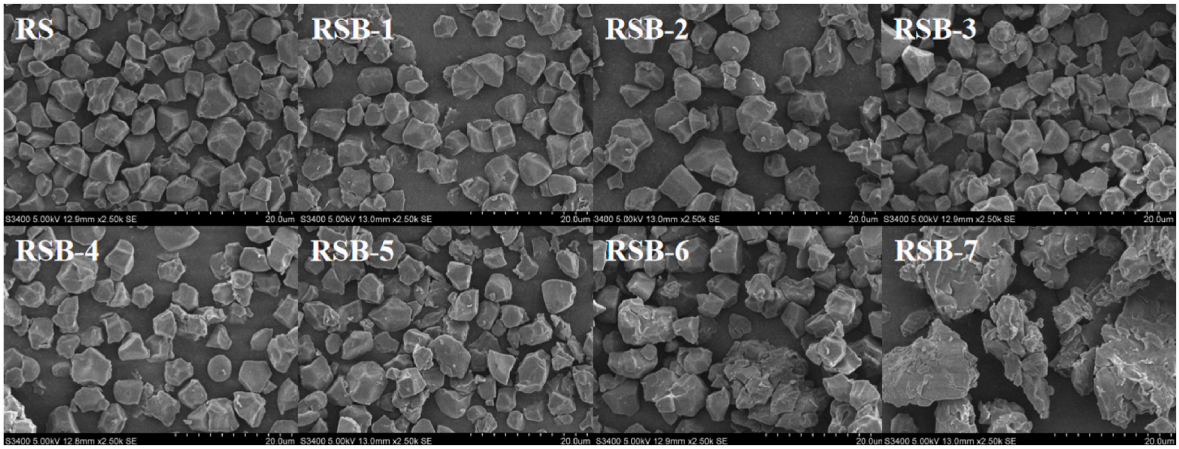

Fig. 3. Morphological changes in natural (RS) and butyrylated (RSB) starches.

Table 3
Pasting parameters of rice starch (RS) and butyrate rice starch (RSB).

Samples	PV (cP)	TV (cP)	BD (cP)	FV (cP)	SB (cP)	PaT (°C)
RS	2687.0 ± 83.9^{a}	2018.0 ± 350.8^{a}	669.0 ± 212.7^{a}	3459.2 ± 233.8^{a}	1441.2 ± 34.7^{a}	71.5 ± 0.8^{e}
RSB-1	1736.7 ± 103.3^{e}	1633.0 ± 212.7^{a}	103.7 ± 135.0^{bc}	854.3 ± 219.0^{f}	221.3 ± 57.5^{c}	79.3 ± 0.5^{d}
RSB-2	1078.0 ± 13.9^{d}	897.0 ± 58.9^{e}	181.0 ± 54.3^{bc}	1452.0 ± 349.1^{cd}	555.0 ± 93.4^{c}	92.3 ± 0.3^{a}
RSB-3	1546.3 ± 25.7^{f}	1438.7 ± 45.0^{b}	107.6 ± 59.4^{c}	647.3 ± 32.7^{d}	196.7 ± 29.6^{bc}	94.5 ± 1.0^{a}
RSB-4	1353.7 ± 23.8^{c}	1181.3 ± 149.7^{bc}	172.7 ± 43.6^{bc}	2033.7 ± 435.5^{b}	208.6 ± 267.9^{b}	83.7 ± 0.4^{a}
RSB-5	1445.0 ± 86.3^{b}	1283.7 ± 76.9^{d}	161.3 ± 38.7^{b}	1846.8 ± 147.9^{b}	563.1 ± 93.0^{b}	89.1 ± 1.3^{c}
RSB-6	1255.3 ± 25.8^{d}	768.5 ± 41.3^{d}	486.8 ± 60.7^{b}	1358.4 ± 46.4^{bc}	589.9 ± 82.5^{bc}	92.4 ± 0.6^{b}
RSB-7	1054.3 ± 45.7^{b}	678.1 ± 56.3^{d}	376.2 ± 67.1^{d}	1045.7 ± 62.8^{de}	367.6 ± 78.3^{bc}	93.7 ± 1.5^{a}

PV: Peak viscosity, TV: Trough viscosity, BD: Breakdown viscosity, FV: Final viscosity, SB: Setback viscosity, PaT: Pasting temperature. All values are means ± SD (n = 3); values with the same letters in the same column do not differ significantly ($p < 0.05$).

2021). The regrowth values exhibited a significant decrease ($p < 0.05$) with increasing levels of substitution, suggesting that the incorporation of butyric acid impeded hydrogen bonding among the linear starch chains, decelerating the retrogradation process of the starches. The temperature at which starch granules achieve maximum swelling is referred to as the pasting temperature. The esterified samples demonstrated a substantially higher pasting temperature compared to the native rice starch. This phenomenon could be attributed to the fact that an increased level of esterification inhibits or prevents the swelling of starch granules, resulting in a higher starch ester pasting temperature (Martins et al., 2018). Similarly, Remya et al. (2018) observed a decrease in viscosity parameters with an increase in the degree of esterification cross-linking with organic acids in the starch molecule. This effect was associated with the crystalline regions of branched starch and the disruption of glycosidic chains. Moreover, Hadi et al. (2024) reported that the incorporation of short-chain fatty acids of varying chain lengths into rice starch led to a reduction in the pasting value. This was consistent with this study's findings.

3.7. Thermal properties

Alterations in the degree of substitution of butyrate result in modifications to the thermal properties of starch. Table 4 described the variation of these thermal properties, including the onset temperature (T_0), peak temperature (T_p), conclusion temperature (T_c), and enthalpy of gelation (ΔH). The T_0 of resistant starch was observed to be higher than that of RSB, aligning with previous research findings (Selma-Gracia et al., 2020). Li et al. (2022d) also corroborated that the T_0 of butylated rice starch decreased with an increase in DS. These variations occur because an increase in DS cause the butyrylation of hydroxyl groups within the starch molecule. This reduction in hydrogen bonding between molecules resulted in a decrease in the pasting temperature (Hadi et al., 2020). With an increase in the degree of substitution, both the pasting temperature and the gelatinization temperature decreased. This phenomenon could be attributed to the incorporation of a butyryl group into the structure of dehydrated glucose, replacing the hydroxyl sites and thereby weakening the hydrogen bonds (Hadi et al., 2020; Li et al., 2022d). The enthalpy change indicates a loss of double helix order rather than a loss of crystallinity. The rearrangement of starch molecules within the double helix configuration requires energy (Wen et al., 2020). Butyric starch esters exhibited a significantly lower heat absorption enthalpy ($P > 0.05$) compared to natural starch. This observation suggested that the substitution of rice starch with butyric acid modifies the amylose chain stacking, leading to an increase in amorphous regions and a consequent reduction in relative crystallinity. These results were consistent with the findings obtained from XRD analysis.

Table 4
Thermal properties of rice starch (RS) and butyrate rice starch (RSB).

Samples	T_0(°C)	T_P(°C)	T_C(°C)	ΔH(J/g)
RS	65.32 ± 0.63^{a}	75.35 ± 1.48^{a}	82.63 ± 2.59^{a}	27.43 ± 1.32^{a}
RSB-1	56.27 ± 1.46^{d}	63.57 ± 1.03^{c}	81.50 ± 0.01^{b}	17.87 ± 0.59^{d}
RSB-2	52.73 ± 1.80^{e}	63.15 ± 0.85^{cd}	80.02 ± 0.97^{b}	13.79 ± 1.56^{f}
RSB-3	55.52 ± 0.93^{c}	63.79 ± 0.16^{c}	81.73 ± 1.81^{ab}	15.76 ± 1.32^{e}
RSB-4	63.64 ± 0.51^{ab}	72.59 ± 0.62^{bc}	80.32 ± 0.43^{c}	20.32 ± 0.15^{b}
RSB-5	61.57 ± 0.72^{b}	74.76 ± 0.63^{b}	80.06 ± 0.72^{b}	19.37 ± 0.87^{c}
RSB-6	63.14 ± 0.20^{ab}	73.34 ± 0.33^{a}	80.71 ± 0.43^{ab}	21.25 ± 0.14^{b}
RSB-7	61.13 ± 0.22^{ab}	74.12 ± 0.13^{a}	80.24 ± 0.23a^{d}	20.77 ± 0.14^{b}

Different superscript letters indicate that the values in each column are significantly different ($p < 0.05$).

3.8. In vitro digestibility

The rapid-digestible starch (RDS), slow-digestible starch (SDS), and resistant starch (RS) contents of rice starch and other butyrate rice starch samples were shown in Fig. 4. The RDS content of raw rice starch was about 37.63%, while the SDS and resistant starch contents were 38.40% and 24.33%, respectively. Following butyric acid treatment, the RDS content of the RSB decreased significantly, whereas the resistant starch content increased from 39.46% to 47.72%. This phenomenon was attributed to the formation of a highly site-blocking structure that impedes enzymatic digestion (Wang et al., 2024). As the degree of substitution increased, there was a notable reduction in the content of RDS and a corresponding increase in the content of resistant starch. This was attributed to the ability of digestive enzymes to effectively hydrolyze the structure of SDS and convert it into resistant starch. Consequently, this modification protected the starch molecules and inhibited enzymatic degradation (Chen et al., 2024b; Dai et al., 2019).

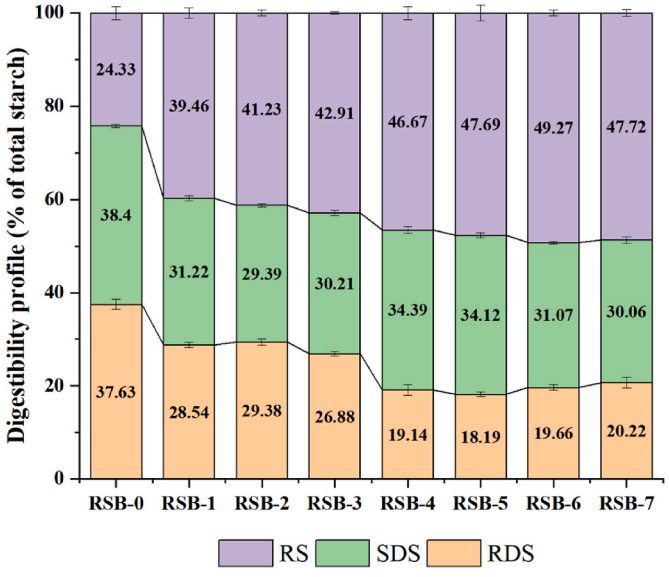

Fig. 4. Rapidly digests starch (RDS), slowly digested starch (SDS) and resistant starch (RS) contents of natural and butyrylated starches.

4. Conclusion

We prepared rice starch-based (RSB) samples with degrees of substitution ranging from 0.047 to 0.206, utilizing crushed rice starch as the starting material. Fourier-transform infrared spectroscopy analysis indicated the emergence of a distinct characteristic peak at 1726 cm^{-1} in the RSB samples, which signifies the successful esterification of rice starch with butyric acid. The esterification processes led to the formation of irregular granular structures, with the observed DS values correlating with these morphological changes. Notably, both RS and RSB samples did not exhibit any new characteristic peaks, suggesting that the A-type crystalline structure of rice starch remained preserved throughout the process. The relative crystallinity of the RS sample exhibited an increase from 24.77% to 8.41%. Additionally, it was observed that with an increase in the DS value, all pasting parameters of RSB were lower compared to those of natural starch. As the degree of substitution in RSB samples increased, the resistant starch content rose from 24.33% to 47.72%, while the RDS and SDS contents decreased. Therefore, RSB has good prospects for application in the food and pharmaceutical fields due to its functional properties.

CRediT authorship contribution statement

Qiaoyan Wu: Conceptualization, Formal analysis, Project administration, Writing – review & editing. **Yang Yang:** Data curation, Validation, Writing – original draft. **Yue Xu:** Data curation, Validation, Writing – original draft. **Bing Wang:** Data curation, Validation, Writing – original draft. **Xiaofei Liu:** Data curation, Methodology, Software. **Yan Wang:** Data curation, Methodology, Software. **Guang Zhang:** Formal analysis, Investigation, Methodology. **Xin Bian:** Formal analysis, Investigation, Methodology. **Chunmin Ma:** Funding acquisition, Project administration, Resources, Supervision. **Na Zhang:** Funding acquisition, Project administration, Resources, Supervision.

Declaration of competing interest

The authors declare that they have no known competing financial interests or personal relationships that could have appeared to influence the work reported in this paper.

Data availability

No data was used for the research described in the article.

Acknowledgments

This work was financially supported by the National Key Research and Development Program of China (2023YFD2100803); National Natural Science Foundation of China (32372387); and Heilongjiang Province Project (2023ZXJ08B03).

References

Ali, T.M., Hasnain, A., 2016. Physicochemical, morphological, thermal, pasting, and textural properties of starch acetates. Food Rev. Int. 322, 161–180. https://doi.org/10.1080/87559129.2015.1057842.

Cao, C., Shen, M., Hu, J., Qi, J., Xie, P., Zhou, Y., 2020. Comparative study on the structure-properties relationships of native and debranched rice starch. CyTA-J. Food 181, 84–93. https://doi.org/10.1080/19476337.2019.1710261xc.

Chen, L., Li, X., Li, W., Hao, X., Wu, S., Zhang, M., Zheng, F., Zhang, N., 2024a. Structural, physicochemical, and digestive properties of enzymatic debranched rice starch modified by phenolic compounds with varying structures. J. Bio. Macrom. 133262. https://doi.org/10.1016/j.ijbiomac.2024.133262.

Chen, W., Li, X., Bodjrenou, D.M., Zhang, Y., Zeng, H., 2024b. Butyryl group distribution modulates the structure and properties of butyrylated maize starch focused on amylose contents. Int. J. Biol. Macromol. 265, 130794. https://doi.org/10.1016/j.ijbiomac.2024.130794.

Cheng, J., Zhou, J., 2024. Unraveling the gut health puzzle: exploring the mechanisms of butyrate and the potential of High-Amylose Maize Starch Butyrate HAMSB in alleviating colorectal disturbances. Front. Nutr. 11, 1285169. https://doi.org/10.3389/fnut.2024.1285169.

Cornejo-Ramírez, Y.I., Martínez-Cruz, O., Del Toro-Sánchez, C.L., Wong-Corral, F.J., Borboa-Flores, J., Cinco-Moroyoqui, F.J., 2018. The structural characteristics of starches and their functional properties. CyTA-J. Food. 161, 1003–1017. https://doi.org/10.1080/19476337.2018.1518343.

Cuenca, P., Ferrero, S., Albani, O., 2020. Preparation and characterization of cassava starch acetate with high substitution degree. Food Hydrocolloids 100, 105430. https://doi.org/10.1016/j.foodhyd.2019.105430.

Dai, D., Sun, S., Hong, Y., Gu, Z., Cheng, L., Li, Z., Li, C., 2019. Structural and functional characteristics of butyrylated maize starch. Lebensm. Wiss. Technol. 112, 108254. https://doi.org/10.1016/j.lwt.2019.108254.

Dhull, S.B., Punia, S., Kumar, M., Singh, S., Singh, P., 2021. Effect of different modifications physical and chemical on morphological, pasting, and rheological properties of black rice Oryza sativa L. Indica starch: a comparative study. Starch Staerke 731–2, 2000098. https://doi.org/10.1002/star.202000098.

Di Filippo, S., Tupa, M.V., Vázquez, A., Foresti, M.L., 2016. Organocatalytic route for the synthesis of propionylated starch. Carbohydr. Polym. 137, 198–206. https://doi.org/10.1016/j.carbpol.2015.10.039.

Diop, C.I.K., Li, H.L., Xie, B.J., Shi, J., 2011. Effects of acetic acid/acetic anhydride ratios on the properties of corn starch acetates. Food Chem. 1264, 1662–1669. https://doi.org/10.1016/j.foodchem.2010.12.050.

Dong, F., Gao, W., Liu, P., Kang, X., Yu, B., Cui, B., 2023. Digestibility, structural and physicochemical properties of microcrystalline butyrylated pea starch with different degree of substitution. Carbohydr. Polym. 314, 120927. https://doi.org/10.1016/j.carbpol.2023.120927.

Egharevba, H.O., 2019. Chemical properties of starch and its application in the food industry. Chem. Prop. Starch 63–72. https://doi.org/10.5772/intechopen.87777.

Espinosa-Solis, V., García-Tejeda, Y.V., Leal-Castañeda, E.J., Barrera-Figueroa, V., 2020. Effect of the degree of substitution on the hydrophobicity, crystallinity, and thermal properties of lauroylated amaranth starch. Polym 1211, 2548. https://doi.org/10.3390/polym12112548.

Fu, X., Liu, Z., Zhu, C., Mou, H., Kong, Q., 2019. Nondigestible carbohydrates, butyrate, and butyrate-producing bacteria. Crit. Rev. Food Sci. Nutr. 59sup1 S130–S152. https://doi.org/10.1080/10408398.2018.1542587.

Gao, W., Sui, J., Liu, P., Cui, B., Abd El-Aty, A.M., 2021. Synthetic mechanism of octenyl succinic anhydride modified corn starch based on shells separation pretreatment. Int. J. Biol. Macromol. 172, 483–489. https://doi.org/10.1016/j.ijbiomac.2021.01.082.

Guo, K., Tian, Y., Podzimska-Sroka, D., Kirkensgaard, J.J.K., Herburger, K., Enemark-Rasmussen, K., Hassenkam, T., Petersen, B.L., Blennow, A., Zhong, Y., 2024. Structural evolution of maize starches with different amylose content during pasting and gelation as evidenced by rapid Visco Analyser. Food Chem. 140817. https://doi.org/10.1016/j.foodchem.2024.140817.

Hadi, N.A., Marefati, A., Purhagen, J., Rayner, M., 2024. Physicochemical and functional properties of short-chain fatty acid starch modified with different acyl groups and levels of modification. Int. J. Biol. Macromol. 267, 131523. https://doi.org/10.1016/j.ijbiomac.2024.131523.

He, J., Zhang, P., Shen, L., Niu, L., Tan, Y., Chen, L., Zhao, Y., Bai, L., Hao, X.X., Li, X.W., Zhang, S.H., Zhu, L., 2020. Short-chain fatty acids and their association with signalling pathways in inflammation, glucose and lipid metabolism. Int. J. Mol. Sci. 2117, 6356–6371. https://doi.org/10.3390/ijms21176356.

Jiang, J., Gao, H., Zeng, J., Zhang, L., Wang, F., Su, T., Li, G., 2021. Determination of subfreezing temperature and gel retrogradation characteristics of potato starch gel. Lebensm. Wiss. Technol. 149, 112037. https://doi.org/10.1016/j.lwt.2021.112037.

Li, L., Cheng, L., Li, Z., Li, C., Hong, Y., Gu, Z., 2021. Butyrylated starch protects mice from DSS-induced colitis: combined effects of butyrate release and prebiotic supply. Food Funct. 1222, 11290–11302. https://doi.org/10.1039/D1FO01913A.

Li, L., Li, W., Yang, L., Cheng, L., Li, Z., Li, C., Hong, Y., Gu, Z., 2022b. Butyl group distribution, intestinal digestion, and colonic fermentation characteristics of different butyrylated starches. J. Agric. Food Chem. 7010, 3289–3299. https://doi.org/10.1021/acs.jafc.1c07861.

Li, M., Wang, J., Wang, F., Wu, M., Wang, R., Strappe, P., Blanchard, C., Zhou, Z., 2022c. Insights into the multi-scale structure of wheat starch following acylation: physicochemical properties and digestion characteristics. Food. Hydrocoll. 124, 107347. https://doi.org/10.1016/j.foodhyd.2021.107347.

Li, X., Chen, W., Bodjrenou, D.M., Huang, M., Zhang, Y., Zheng, B., Zeng, H., 2022d. Properties of butyrylated lotus seed starch with butyryl groups at different carbon positions. Carbohydr. Polym. 294, 119766. https://doi.org/10.1016/j.carbpol.2022.119766.

Li, X., Gao, J., Chen, W., Liang, J., Gao, W., Bodjrenou, D.M., Zeng, H., Zhang, Y., Farag, M.A., Cao, H., Zheng, B., 2024. Properties and functions of acylated starch with short-chain fatty acids: a comprehensive review. Crit. Rev. Food Sci. Nutr. 1–14. https://doi.org/10.1080/10408398.2024.2365343.

Liu, Y., Gao, J., Wu, H., Gou, M., Jing, L., Zhao, K., Zhang, B., Zhang, g., Li, W., 2019. Molecular, crystal and physicochemical properties of granular waxy corn starch after repeated freeze-thaw cycles at different freezing temperatures. Int. J. Biol. Macromol. 133, 346–353. https://doi.org/10.1016/j.ijbiomac.2019.04.111.

Ma, Z., Boye, J.I., 2018. Research advances on structural characterization of resistant starch and its structure-physiological function relationship: a review. Crit. Rev. Food Sci. Nutr. 58 (7), 1059–1083. https://doi.org/10.1080/10408398.2016.1230537.

Maiuolo, J., Bulotta, R.M., Ruga, S., Nucera, S., Macrì, R., Scarano, F., Oppedisano, F., Carresil, C., Gliozzil, M., Musolino, V., Mollace, R., Muscoli, C., Mollace, V., 2024. The postbiotic properties of butyrate in the modulation of the gut microbiota: the potential of its combination with polyphenols and dietary fibers. Int. J. Mol. Sci. 2513, 6971–6996. https://doi.org/10.3390/ijms25136971.

Martins, P.C., Gutkoski, L.C., Martins, V.G., 2018. Impact of acid hydrolysis and esterification process in rice and potato starch properties. Int. J. Biol. Macromol. 120, 959–965. https://doi.org/10.1016/j.ijbiomac.2018.08.170.

Portillo-Perez, G.A., Skov, K.B., Martinez, M.M., 2024. Starch esterification using deep eutectic solvents as chaotropic agents and reaction promoters. Green Chem. 264, 2225–2240. https://doi.org/10.1039/D3GC02833J.

Portincasa, P., Bonfrate, L., Vacca, M., De Angelis, M., Farella, I., Lanza, E., Khalil, M., Wang, D.Q.H., Sperandio, M., Di Ciaula, A., 2022. Gut microbiota and short chain fatty acids: implications in glucose homeostasis. Int. J. Mol. Sci. 233, 1105–1131. https://doi.org/10.3390/ijms23031105.

Remya, R., Jyothi, A.N., Sreekumar, J., 2018. Effect of chemical modification with citric acid on the physicochemical properties and resistant starch formation in different starches. Carbohydr. Polym. 202, 29–38. https://doi.org/10.1016/j.carbpol.2018.08.128.

Rostamabadi, H., Nowacka, M., Kumar, Y., Xu, S., Colussi, R., Frasson, S.F., Singh, S.K., Falsafi, S.R., 2024a. Green modification techniques: sustainable approaches to induce novel physicochemical and technofunctional attributes in legume starches. Trends Food Sci. Technol. 104389. https://doi.org/10.1016/j.tifs.2024.104389.

Rostamabadi, H., Yildirim-Yalcin, M., Demirkesen, I., Toker, O.S., Colussia, R., do Nascimentob, L.Á., Sahin, S., Falsafi, S.R., 2024b. Improving physicochemical and nutritional attributes of rice starch through green modification techniques. Food Chem. 140212. https://doi.org/10.1016/j.foodchem.2024.140212.

Selma-Gracia, R., Laparra, J.M., Haros, C.M., 2020. Potential beneficial effect of hydrothermal treatment of starches from various sources on in vitro digestion. Food. Hydrocoll 103, 105687. https://doi.org/10.1016/j.foodhyd.2020.105687.

Shi, C., Zhu, S., Du, C., Zhong, F., Huang, D., Li, Y., 2022. Octenylsuccinic anhydride group distribution in esterified maize starches with different granular structure and its effect on starch digestibility. Food Biosci. 50, 102056. https://doi.org/10.1016/j.fbio.2022.102056.

Sinhmar, A., Pathera, A.K., Sharma, S., Nehra, M., Thory, R., Nain, V., 2023. Impact of various modification methods on physicochemical and functional properties of starch: a review. Starch Staerke 751–2, 2200117. https://doi.org/10.1002/star.202200117.

Su, H., Tu, J., Zheng, M., Deng, K., Miao, S., Zeng, S., Zheng, B., Lu, X., 2020. Effects of oligosaccharides on particle structure, pasting and thermal properties of wheat starch granules under different freezing temperatures. Food Chem. 315, 126209. https://doi.org/10.1016/j.foodchem.2020.126209.

Wang, M., Wichienchot, S., He, X., Fu, X., Huang, Q., Zhang, B., 2019. In vitro colonic fermentation of dietary fibers: fermentation rate, short-chain fatty acid production and changes in microbiota. Trends Food Sci. Technol. 88, 1–9. https://doi.org/10.1016/j.tifs.2019.03.005.

Wang, Y., Tao, L., Wang, Z., Wang, Y., Lin, X., Dai, J., Shi, C., Dai, T., Sheng, J., Tian, Y., 2024. Effect of succinylation-assisted glycosylation on the structural characteristics, emulsifying, and gel properties of walnut glutenin. Food Chem. 446, 138856. https://doi.org/10.1016/j.foodchem.2024.138856.

Wang, Z., Wang, L., Yu, X., Wang, X., Zheng, Y., Hu, X., Zhao, P., Sun, Q., Wang, Q., Li, N., 2024. Effect of polysaccharide addition on food physical properties: a review. Food Chem. 431, 137099. https://doi.org/10.1016/j.foodchem.2023.137099.

Wen, Y., Yao, T., Xu, Y., Corke, H., Sui, Z., 2020. Pasting, thermal and rheological properties of octenylsuccinylate modified starches from diverse small granule starches differing in amylose content. J. Cereal. S. 95, 103030. https://doi.org/10.1016/j.jcs.2020.103030.

Xie, Z., Wang, S., Wang, Z., Fu, X., Huang, Q., Yuan, Y., Wang, K., Zhang, B., 2019. In vitro fecal fermentation of propionylated high-amylose maize starch and its impact on gut microbiota. Carbohydr. Polym. 223, 115069. https://doi.org/10.1016/j.carbpol.2019.115069.

Xu, Q., Ma, R., Zhan, J., Lu, X., Liu, C., Tian, Y., 2023. Acylated resistant starches: changes in structural properties during digestion and their fermentation characteristics. Food Hydrocolloids 139, 108578. https://doi.org/10.1016/j.foodhyd.2023.108578.

Yao, Y., Cai, X., Fei, W., Ye, Y., Zhao, M., Zheng, C., 2022. The role of short-chain fatty acids in immunity, inflammation and metabolism. Crit. Rev. Food Sci. Nutr. 621, 1–12. https://doi.org/10.1080/10408398.2020.1854675.

Zarski, A., Kapusniak, K., Ptak, S., Rudlicka, M., Coseri, S., Kapusniak, J., 2024. Functionalization methods of starch and its derivatives: from old limitations to new possibilities. Polym 165, 597–623. https://doi.org/10.3390/polym16050597.

Zhang, Y., Li, L., Sun, S., Cheng, L., Gu, Z., Hong, Y., 2024. Structural characteristics, digestion properties, fermentation properties, and biological activities of butyrylated starch: a review. Carbohydr. Polym. 121825. https://doi.org/10.1016/j.carbpol.2024.121825.

Zhao, K., Li, B., Xu, M., Jing, L., Gou, M., Yu, Z., Zheng, J., Li, W., 2018. Microwave pretreated esterification improved the substitution degree, structural and physicochemical properties of potato starch esters. Lebensm. Wiss. Technol. 90, 116–123. https://doi.org/10.1016/j.lwt.2017.12.021.